Satellite band structure in silicon caused by electron-plasmon coupling

Johannes Lischner, G. K. Pálsson, Derek Vigil-Fowler, S. Nemsak, J. Avila, M. C. Asensio, C. S. Fadley, and Steven G. Louie

Satellite Band Structure in Silicon Caused by Electron-Plasmon Coupling

Johannes Lischner,[1, *] G. K. Pálsson,[2] Derek Vigil-Fowler,[1] S. Nemsak,[2]
J. Avila,[3] M. C. Asensio,[3] C. S. Fadley,[2] and Steven G. Louie[1]

[1] *Department of Physics, University of California, Berkeley,*
California 94720, USA, and Materials Sciences Division,
Lawrence Berkeley National Laboratory, Berkeley 94720, USA.
[2] *Department of Physics, University of California, Davis,*
California 95616, USA, and Materials Sciences Division,
Lawrence Berkeley National Laboratory, Berkeley 94720, USA.
[3] *Synchrotron SOLEIL, Saint Aubin, BP 48 91192 Gif-sur-Yvette, France*

We report the first angle-resolved photoemission measurement of the wave-vector dependent plasmon satellite structure of a three-dimensional solid, crystalline silicon. In sharp contrast to nanomaterials, which typically exhibit strongly wave-vector dependent, low-energy plasmons, the large plasmon energy of silicon facilitates the search for a plasmaron state consisting of resonantly bound holes and plasmons and its distinction from a weakly interacting plasmon-hole pair. Employing a first-principles theory, which is based on a cumulant expansion of the one-electron Green's function and contains significant electron correlation effects, we obtain good agreement with the measured photoemission spectrum for the wave-vector dependent dispersion of the satellite feature, but without observing the existence of plasmarons in the calculations.

Introduction. — Within the contemporary view of condensed matter physics[1] in the Fermi liquid paradigm, the electronic structure of materials is described in terms of a quasiparticle picture, where particle-like excitations (such as those measured in transport or photoemission experiments) in an otherwise strongly interacting electron system are characterized by weakly interacting quasi-electrons and quasi-holes, consisting of the bare particles and a surrounding screening cloud of electron-hole pairs and collective excitations. One example of such collective excitations are plasmons, quantized charge density oscillations resulting from the long-range nature of the Coulomb interaction. Both the energy and the dispersion relation of plasmons depend sensitively on the dimensionality of the material. In three-dimensional materials, the energy required to excite a plasmon is typically multiple electron volts, but in two- and one-dimensional systems, such as doped graphene[2] or metallic carbon nanotubes[3], plasmons can be gapless excitations with strong wave-vector dependence and vanishing energy in the zero wave-vector limit.

The interaction with plasmons has an important effect on the properties of electrons and holes in solids. For example, the energy dispersion relation of the electrons in a crystal (the band structure) is modified. As a more drastic consequence of strong electron-plasmon coupling, Lundqvist[4] predicted the emergence of a new kind of composite quasiparticles, called plasmarons [5], consisting of resonantly bound plasmons and holes, which give rise to additional sharp features from the conventional quasiparticle peaks, known as the satellite structures, in photoemission and tunneling spectra. Recent experiments on doped graphene[6–8] and two-dimensional elec-

tron gases in semiconductor quantum wells[9] observed prominent satellite structures, which were interpreted as signatures of plasmaron excitations.

Other studies[10, 11] pointed out that the observed satellite features could also result from the creation of weakly interacting plasmon-hole pairs instead of strongly interacting plasmaron states. Such shake-up satellites are well known in the photoemission spectroscopy of molecules, where they result from the creation of an electron-hole pair or a vibrational mode in addition to the quasi-hole in the photo-excitation process. Because of the low plasmon energy in two-dimensional systems (which is proportional to the square root of the plasmon wave vector) and other experimental complications, such as the dielectric screening from a substrate, it has been difficult to identify unambiguously from experiment whether the observed satellites originate from plasmarons or shake-up processes involving plasmons.

In three-dimensional systems, the plasmon energy is much larger than in two- and one-dimensional systems (it approaches a large constant value at small wave vectors plus a term which is proportional to the square of the plasmon wave vector) resulting in significant energy differences between possible plasmaron states and unbound hole-plasmon pairs. Also, possible complications from environmental screening are eliminated. However, obtaining angle-resolved photoemission spectra of bulk satellite features requires higher energy photons because of the higher binding energy of the satellites and also the need to minimize surface related effects. So far, satellite properties in three-dimensional solids were only probed in angle-integrated photoemission experiments[12, 13], but such experiments do not give direct insights into satellite
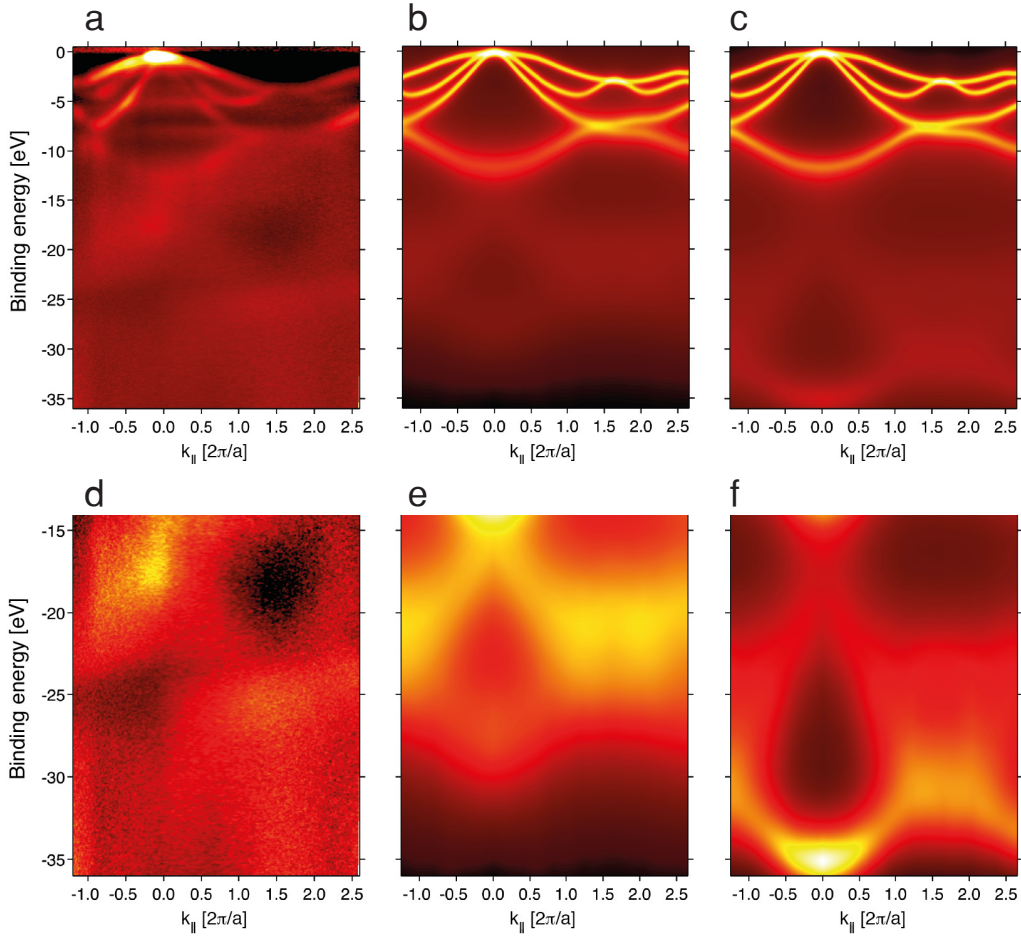
FIG. 1. (a): Experimental photoemission spectrum of silicon taken along $\phi = -30°$ (see appendix for definition of ϕ) using a photon energy of 711 eV. Here, $k_{||}$ denotes the component of electron wave vector parallel to the surface. (b) and (c): Theoretical photoemission spectra from GW plus cumulant theory and GW theory, respectively along $\phi = -30°$. (d), (e) and (f): Same spectra as in (a), (b) and (c), but only the binding energy range relevant to the first satellite feature is shown.

properties associated with individual quasiparticle states, such as their line widths and dispersions.

To elucidate the nature of the plasmon satellites in three-dimensional solids, we chose silicon as a prototypical system. It is one of the most studied and technologically important three-dimensional semiconductor materials, and a full understanding of its electronic structure including the wave-vector dependent satellite properties is highly desirable. Accurate knowledge of the electron-plasmon and light-plasmon interactions is particularly important for current and future plasmonic devices[14–16].

Results—. Figure 1(a) shows the measured angle-resolved photoemission spectrum from the [111] surface of silicon along the $\phi = -30°$ direction (see appendix) using photons with an energy of 711 eV. The spectrum exhibits prominent sharp, dispersive features at binding energies smaller than 13 eV corresponding to the usual quasiparticle excitations (i.e., the band states). At binding energies higher than 15 eV, we observe a more diffuse

satellite band structure, which looks like a fainter, broadened copy of the quasiparticle band structure. Figure 2(a) shows the measured angle-resolved photoemission spectrum along the $\phi = -60°$ direction and exhibits similar features to the spectrum obtained along $\phi = -30°$.

To gain insight into the observed photoemission spectra, we compare them to state-of-the-art theories of electronic excitations in condensed matter systems. Such theories yield spectral functions, $A_{n\boldsymbol{k}}(\omega) = 1/\pi \times |\mathrm{Im}G_{n\boldsymbol{k}}(\omega)|$, which are proportional to the angle-resolved photoemission spectrum within the sudden approximation[17]. Here, n and $\boldsymbol{k}$ are the band index and the wave vector of the hole created in the photoemission process, respectively, and $G_{n\boldsymbol{k}}(\omega)$ denotes the wave vector and frequency-dependent interacting one-particle Green's function. Calculations of the Green's function typically proceed by evaluating a set of Feynman diagrams, which represent interaction processes between the electrons and other excitations[18].

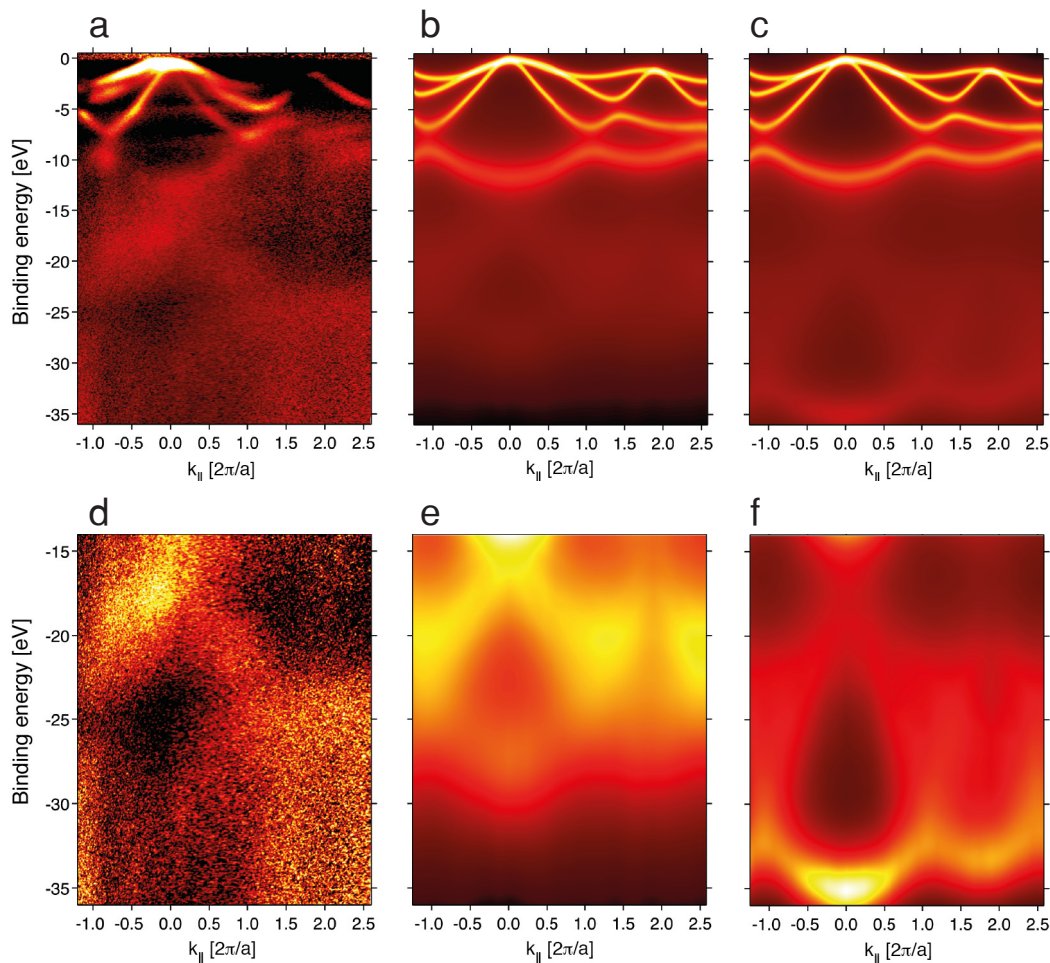The GW method[19, 20] has been used to analyze pho-

FIG. 2. (a): Experimental photoemission spectrum along $\phi = -60^\circ$ (see appendix for a description of the experimental photoemission setup). (b) and (c): Theoretical photoemission spectra from GW plus cumulant theory and GW theory, respectively. (d), (e) and (f): Same spectra as in (a), (b) and (c), but only the binding energy range relevant to the first satellite is shown.

toemission experiments and, recently, to interpret satellite features for two-dimensional systems[6, 7, 9]. This approach captures the complicated, dynamic polarization response of the electron sea to the appearance of a hole in the photoemission process by approximating the electron self-energy as the first term in a Feynman series expansion in the screened Coulomb interaction, but it neglects the contribution of other higher order Feynman diagrams describing additional correlation effects between electrons. For low-energy quasiparticle properties, such as the electronic band gaps and quasiparticle dispersion relations of semiconductors and insulators, the GW approach has resulted in very good agreement with experimental measurements from first principles[20]. However, much less is known about its accuracy for satellite properties. For the special case of a dispersionless hole (such as the hole resulting from the removal of an electron from a tightly bound atomic core state) interacting with plasmons, the GW approach fails dramatically to describe the satellite properties[10, 12, 21]. The exact solution of

this model problem can be obtained using a cumulant expansion of the Green's function[22]. The resulting spectral function exhibits an infinite series of satellite peaks, separated by the plasmon energy from the quasiparticle peak and from each other. The GW approach instead predicts a single satellite peak separated from the quasiparticle peak by 1.5 plasmon energies[23]. This demonstrates that theories containing additional correlation effects beyond GW theory can give rise to qualitatively different predictions for the satellites.

The first-principles GW plus cumulant (GW+C) approach[10] we use in the present study is a means to generalize the exact solution of the core electron problem to the case of dispersing valence electrons[21, 24]. It retains the accuracy of the first-principles GW approach for quasiparticle properties, but includes approximately an infinite number of higher order diagrams, which are needed for an accurate description of satellite properties.

Figures 1(b) and (c) show the calculated photoemission spectra from the GW plus cumulant (GW+C) and

GW approaches, respectively, for the $\phi = -30°$ direction. Both theories predict prominent, intense, occupied quasiparticle bands at binding energies smaller than 13 eV and a less intense satellite band structure at higher binding energies. While the satellite band structures obtained from the GW and GW+C methods look qualitatively similar, there are several significant differences: (i) the binding energy of the satellite bands is significantly larger in the GW method extending to more than 35 eV, while the GW plus cumulant satellite bands only extend to less than 30 eV, (ii) the total width of the satellite band manifold is 14.4 eV in the GW approach, significantly larger than the GW plus cumulant theory width of 10.8 eV and also the quasiparticle band width of 11.7 eV, and (iii) the distribution of spectral weight is different in the two approaches. In particular, in the GW approach, the highest-binding-energy satellite band at 35 eV binding energy in the vicinity of the Γ-point is very sharp and intense, while the three degenerate satellite bands at lower binding energy are broader and less intense. The GW+C approach does not predict such a sharp, intensive high-binding-energy satellite band.

Discussion—. The sharp satellite band at high binding energies in the GW theory arises from a plasmaron excitation. Mathematically, well-defined excitations result from solutions of the quasiparticle or Dyson's equation, $\omega - \epsilon_{n\boldsymbol{k}} = \Sigma_{n\boldsymbol{k}}(\omega) - V_{n\boldsymbol{k}}^{xc}$, where $\epsilon_{n\boldsymbol{k}}$ denotes the energy obtained from a mean-field calculation, such as a density-functional theory calculation, and $V_{n\boldsymbol{k}}^{xc}$ denotes the corresponding exchange-correlation potential. Here, $\Sigma_{n\boldsymbol{k}}(\omega)$ denotes the self-energy, which describes the interaction of the quasi-hole with plasmons and other excitations. Figure 3(a) shows the graphical solution of the quasiparticle equation for the Γ-point of the bulk Brillouin zone of silicon. If the GW approximation is used to calculate the self-energy[19, 20], we find two solutions: one solution at low binding energy corresponding to a quasiparticle excitation and a second solution at a binding energy of 35 eV corresponding to a plasmaron. In contrast, we do not find a second solution to the Dyson's equation in the GW plus cumulant theory. Figure 3(b) shows that the spectral function from GW plus cumulant theory nevertheless has a second peak, which is separated from the quasiparticle peak by 16 eV. This separation agrees well with the calculated and experimentally measured plasmon energy in silicon[25], indicating that the satellite results from the creation of weakly interacting, unbound plasmon-hole pairs. In particular, it can be shown that the matrix-element weighted density of states of non-interacting hole-plasmon pairs with a particular wave-vector $\boldsymbol{k}$ has a maximum at the sum of the energy of the hole with wave vector $\boldsymbol{k}$ and the zero wave-vector plasmon energy, if both the hole and the plasmon have parabolic dispersion relations; and consequently the satellite band is simply a copy of the hole band shifted by the zero wave-vector plasmon energy. In contrast, the
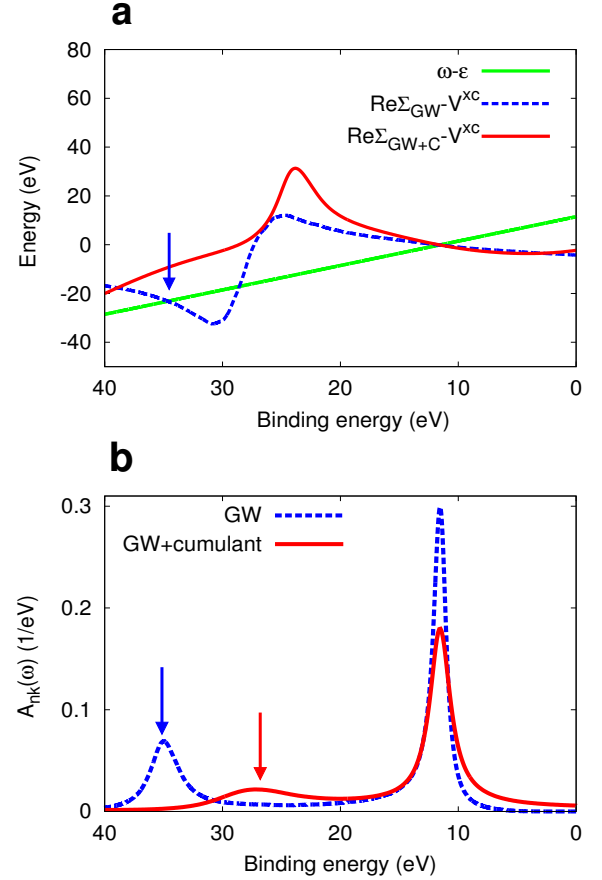
FIG. 3. (a): Graphical solution of Dyson's equation for the lowest valence band of silicon at the Γ-point. The blue arrow denotes the plasmaron solution of the GW theory. (b): Spectral functions for the lowest valence band of silicon at the Γ-point from GW plus cumulant and GW theory. Arrows denote the position of the satellite peaks.

separation in the GW theory is 24 eV, indicating strong interactions between the hole and the plasmons within this lower-order approximation.

Comparing the theoretical spectral functions of the GW and the GW+C approaches to the experimental angle-resolved photoemission spectra (Figures 1 and 2), we find good agreement in both kinds of calculations for the quasiparticle band structure at binding energies smaller than 13 eV. However, for the satellite band structure, the agreement of experiment with GW plus cumulant theory is much better than that with the GW theory. In particular, the experimental spectrum does not show a sharp plasmaron band as satellite at 35 eV, in stark contrast with the prediction of GW theory. Also, the binding energy and the intensities of the measured satellite bands are in good agreement with the GW plus cumulant approach, indicating that the satellite band results from weakly interacting plasmon-hole pairs, very much as is observed in core-level shake-up plasmon satellites[22, 26], but of course with the addition of wave-vector dispersion.

This shows clearly that the observed satellite structures originate from the shake-up of plasmons and not from the formation of plasmarons. Taking into account the good agreement of recent GW+C calculations with spectroscopic measurements in nanomaterials[10, 11], we conclude that the GW+C method provides a unified picture of electron-plasmon interactions in materials. This work also calls into question some prior studies in which plasmarons have been invoked as relevant excitations [6, 7, 9]. Future work should investigate the importance of higher-order cumulant functions which so far have only been studied for electron-phonon interactions[27].

Appendix

Experimental and computational methods.— As a substrate, we used a silicon wafer sufficiently conducting (n-doped, 10-20 Ω·cm) in order to avoid charging effects in the photoemission experiments. The single crystals were cut ($\pm0.05°$) and polished by Siltronix, with the surface oriented perpendicular to the [111]-direction. The sample was introduced into an UHV chamber at a base pressure of $\leq 1 \times 10^{-11}$ mbar and degassed at T = 650 C for 24 hours. The crystal was then repeatedly flash-heated up to T = 1373 C for a few seconds by direct current heating. During flash-heating the pressure remained below p = 5×10^{-9} mbar. This procedure removed the native oxide layer from the surface and resulted in the equilibrium structure of Si(111), the well-known 7×7-reconstruction. This procedure ensured an atomically flat surface, which is the ideal starting condition for an ARPES experiment. To obtain greater bulk sensitivity and minimize the effects from surface states, a photon energy of 711 eV was chosen. The photoemission measurements were performed at liquid nitrogen temperatures to reduce the effects of thermal diffuse scattering, which led to x-ray photoelectron diffraction effects superimposed on the measured ARPES spectra. These effects, although still present in the data, were further separated out using the procedure in of Bostwick and coworkers[6]. The experiments were performed at the ANTARES beam line at the Soleil synchrotron in Paris[28], France, which employs two X-ray undulators in tandem, a PGM monochromator combined with a Scienta R4000 spectrometer. The spectrometer was operated in an angular mode spanning a 25 or 14 degree angular range with a resolution of 0.1 degrees. The angle between the spectrometer and the photon beam was 45 degrees and all spectra were recorded at normal emission. The spectrometer resolution was better than 400 meV at pass energy 200 eV and the photon resolution was 100 meV at hν = 711 eV, yielding an overall instrumental resolution of 130 meV. The binding energy scale was calibrated using the Au 4f$_{7/2}$ peaks at 84.00 eV of a gold reference sample.

For the full-frequency GW calculations for silicon, we used the BerkeleyGW package[29]. For the starting mean-field solution, we carried out density-functional theory (DFT) calculations within the local density approximation (LDA) using a norm conserving pseudopotential with a 45 Ry cutoff and an 8×8×8 k-point grid as implemented in the QUANTUM ESPRESSO program package[30]. In the GW calculations, we calculated the frequency-dependent dielectric matrix in the random phase approximation (RPA) using 96 empty states and a 5 Ry dielectric cutoff. We sampled frequencies using a fine grid with a spacing of 0.2 eV up to 150 eV and then a coarser grid up to 300 eV.

To describe the final state of the photoelectron, we have employed a free electron model based upon an inner potential of 12.5 eV, an average binding energy of 6 eV, and allowance for the work function of the spectrometer. We have also included effects from the non-negligible photon momentum. The resulting set of final-state wave vectors is shown in Fig. 4(b) of the manuscript as the red arc, which represents the span of the detector in the first Brillouin zones after translation by the appropriate reciprocal lattice vector $\boldsymbol{G}_{hkl}$. Note that $\boldsymbol{k} = 0$ in the spectra corresponds to the Γ-point of the bulk Brillouin zone, where the three highest valence bands are degenerate. Matrix element effects were included by using tabulated atomic cross sections and projections of the valence band wave functions onto atomic orbitals.

First-principles GW plus cumulant theory.— In the GW plus cumulant theory[21, 24], the Green's function for a hole is expressed as

$$G_{n\boldsymbol{k}}(t) = i\Theta(-t)\exp\left\{-\frac{i\epsilon_{n\boldsymbol{k}}t}{\hbar} + C_{n\boldsymbol{k}}(t)\right\}, \quad (1)$$

where $\epsilon_{n\boldsymbol{k}}$ denotes the orbital energy from a given mean-field theory (in this work, a density-functional theory
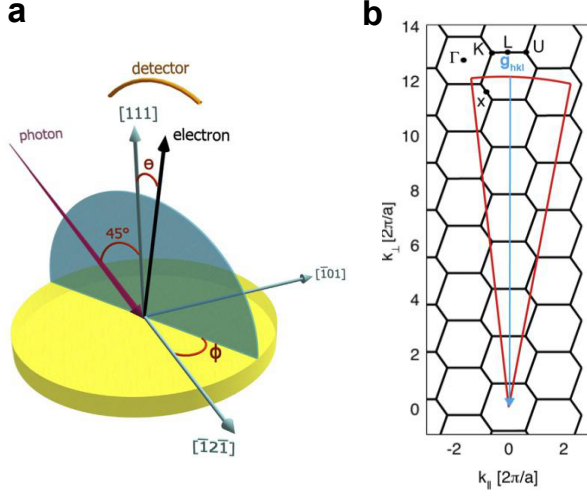
FIG. 4. (a): Real space geometry of the photoemission measurement. (b): Final-state wave vectors of electrons (red line) that reach the detector. The high symmetry points of the Brillouin zone of silicon are labeled.

starting point is employed) and $C_{n\bm{k}}(t)$ denotes the cumulant function. This expression for the Green's function is obtained after the first iteration of the self-consistent solution of its equation of motion assuming a simple quasiparticle form for the starting guess.

The cumulant function can be separated into a quasiparticle part $C_{n\bm{k}}^{qp}(t)$ and a satellite part $C_{n\bm{k}}^{sat}(t)$ given formally in terms of the self energy $\Sigma_{n\bm{k}}(\epsilon)$ by (for $t < 0$)

$$C_{n\bm{k}}^{qp}(t) = -\frac{it\Sigma_{n\bm{k}}(E_{n\bm{k}})}{\hbar} + \frac{\partial \Sigma_{n\bm{k}}^{h}(E_{n\bm{k}})}{\partial \epsilon} \quad (2)$$

$$C_{n\bm{k}}^{sat}(t) = \frac{1}{\pi} \int_{-\infty}^{\mu} d\epsilon \frac{\mathrm{Im}\Sigma_{n\bm{k}}(\epsilon)}{(E_{n\bm{k}} - \epsilon - i\eta)^2} e^{i(E_{n\bm{k}}-\epsilon)t/\hbar}, \quad (3)$$

where μ denotes the chemical potential, η is a positive infinitesimal, $E_{n\bm{k}} = \epsilon_{n\bm{k}} + \Sigma_{n\bm{k}}(E_{n\bm{k}}) - V_{n\bm{k}}^{xc}$ is the quasiparticle energy, and $\Sigma_{n\bm{k}}(\epsilon)$ is defined through the relation

$$\Sigma_{n\bm{k}}^{h}(\epsilon) = \frac{1}{\pi} \int_{-\infty}^{\mu} d\epsilon' \frac{\mathrm{Im}\Sigma_{n\bm{k}}(\epsilon')}{\epsilon' - \epsilon - i\eta}. \quad (4)$$

For a given level of approximation of Σ, the cumulant theory yields an improved Green's function through the above equations. In this work, we employ the first-principles GW approximation[4, 20] for the self energy, which gives accurate quasiparticle properties for a wide range of weakly and moderately correlated semiconductors and insulators.

Having calculated the GW plus cumulant Green's function from the above set of equations, we obtain the corresponding self energy by inverting the Dyson equation

$$\Sigma_{n\bm{k}}^{GW+C}(\epsilon) - V_{n\bm{k}}^{xc} = \epsilon - \epsilon_{n\bm{k}} + i\eta - G_{n\bm{k}}^{-1}(\epsilon). \quad (5)$$
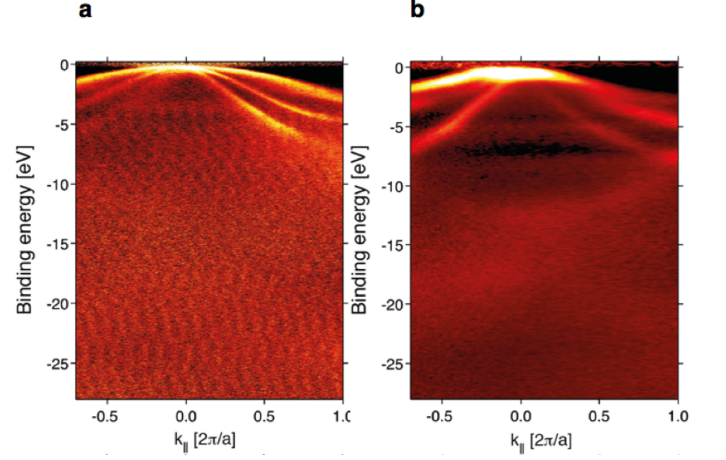

FIG. 5. Comparison of the angle-resolved photoemission spectrum of silicon at different photon energies. Photon energies of 129 eV (a) and 711 eV (b) were used.

Angle-resolved photoemission spectrum at 129 eV photon energy.— We have also measured the angle-resolved photoemission spectrum of silicon at a photon energy of 129 eV. Fig. 5 compares the resulting measured spectrum with the spectrum obtained with 711 eV photons. Although still present at the lower photon energy, the plasmon satellite features are much weaker - a consequence of the reduced extrinsic plasmon losses.

* jlischner597@gmail.com
[1] S. G. Louie and M. L. Cohen, *Conceptual foundations of materials: a standard model for ground- and excited-state properties*, Vol. 2 (Elsevier, 2006).
[2] L. Ju, B. Geng, J. Horng, C. Girit, M. Martin, Z. Hao, H. A. Bechtel, X. Liang, A. Zettl, Y. R. Shen, *et al.*, Nature Nanotechnology **6**, 630 (2011).
[3] M. Lin, D. Chuu, and K.-K. Shung, Physical Review B **56**, 1430 (1997).
[4] L. Hedin, B. Lundqvist, and S. Lundqvist, Solid State Communications **5**, 237 (1967).
[5] To avoid confusion, we point out that the term "plasmaron" has also been used to describe coupled plasmon-phonon states, see for example H. Yu and J. C. Hermanson, Phys. Rev. B 40, 11851 (1989).
[6] A. Bostwick, F. Speck, T. Seyller, K. Horn, M. Polini, R. Asgari, A. H. MacDonald, and E. Rotenberg, Science **328**, 999 (2010).
[7] A. L. Walter, A. Bostwick, K.-J. Jeon, F. Speck, M. Ostler, T. Seyller, L. Moreschini, Y. J. Chang, M. Polini, R. Asgari, *et al.*, Physical Review B **84**, 085410 (2011).
[8] V. W. Brar, S. Wickenburg, M. Panlasigui, C.-H. Park, T. O. Wehling, Y. Zhang, R. Decker, Ç. Girit, A. V. Balatsky, S. G. Louie, *et al.*, Physical Review Letters **104**, 036805 (2010).
[9] O. E. Dial, R. C. Ashoori, L. N. Pfeiffer, and K. W.

West, Phys. Rev. B **85**, 081306(R) (2012).

[10] J. Lischner, D. Vigil-Fowler, and S. G. Louie, Physical Review Letters **110**, 146801 (2013).

[11] J. Lischner, D. Vigil-Fowler, and S. G. Louie, Physical Review B **89**, 125430 (2014).

[12] M. Guzzo, G. Lani, F. Sottile, P. Romaniello, M. Gatti, J. J. Kas, J. J. Rehr, M. G. Silly, F. Sirotti, and L. Reining, Phys. Rev. Lett. **107**, 166401 (2011).

[13] L. Ley, S. Kowalczyk, R. Pollak, and D. Shirley, Physical Review Letters **29**, 1088 (1972).

[14] R. J. Walters, R. V. van Loon, I. Brunets, J. Schmitz, and A. Polman, Nature Materials **9**, 21 (2010).

[15] L. H. Gabrielli, J. Cardenas, C. B. Poitras, and M. Lipson, Nature Photonics **3**, 461 (2009).

[16] S. Pillai, K. Catchpole, T. Trupke, and M. Green, Journal of applied physics **101**, 093105 (2007).

[17] A. Damascelli, Z. Hussain, and Z.-X. Shen, Rev. Mod. Phys. **75**, 473 (2003).

[18] R. D. Mattuck, *A guide to Feynman diagrams in the many-body problem* (Courier Corporation, 2012).

[19] L. Hedin and S. Lundqvist, Solid State Physics **23**, 1 (1969).

[20] M. S. Hybertsen and S. G. Louie, Phys. Rev. B **34**, 5390 (1986).

[21] F. Aryasetiawan, L. Hedin, and K. Karlsson, Phys. Rev. Lett. **77**, 2268 (1996).

[22] D. C. Langreth, Phys. Rev. B **1**, 471 (1970).

[23] B. Lundqvist, Physik der kondensierten Materie **9**, 236 (1969).

[24] L. Hedin, Physica Scripta **21**, 477 (1980).

[25] H. R. Philipp and H. Ehrenreich, Phys. Rev. **129**, 1550 (1963).

[26] R. Baird, C. Fadley, S. Goldberg, P. J. Feibelman, and M. Šunjić, Surface Science **72**, 495 (1978).

[27] O. Gunnarsson, V. Meden, and K. Schönhammer, Phys. Rev. B **50**, 10462 (1994).

[28] J. Avila, I. Razado-Colambo, S. Lorcy, B. Lagarde, J.-L. Giorgetta, F. Polack, and M. C. Asensio, in *Journal of Physics: Conference Series*, Vol. 425 (IOP Publishing, 2013) p. 192023.

[29] J. Deslippe, G. Samsonidze, D. A. Strubbe, M. Jain, M. L. Cohen, and S. G. Louie, Comput. Phys. Commun. **183**, 1269 (2012).

[30] P. Giannozzi, S. Baroni, N. Bonini, M. Calandra, R. Car, C. Cavazzoni, D. Ceresoli, G. L. Chiarotti, M. Cococcioni, I. Dabo, A. Dal Corso, S. de Gironcoli, S. Fabris, G. Fratesi, R. Gebauer, U. Gerstmann, C. Gougoussis, A. Kokalj, M. Lazzeri, L. Martin-Samos, N. Marzari, F. Mauri, R. Mazzarello, S. Paolini, A. Pasquarello, L. Paulatto, C. Sbraccia, S. Scandolo, G. Sclauzero, A. P. Seitsonen, A. Smogunov, P. Umari, and R. M. Wentzcovitch, J. Phys.: Condens. Matter **21**, 395502 (2009).